

Valence bond phases of herbertsmithite and related copper kagome materials

M. R. Norman¹, N. J. Laurita^{2,3} and D. Hsieh^{2,3}¹Materials Science Division, Argonne National Laboratory, Argonne, Illinois 60439, USA²Department of Physics, California Institute of Technology, Pasadena, California 91125, USA³Institute for Quantum Information and Matter, California Institute of Technology, Pasadena, California 91125, USA

(Received 30 October 2019; revised manuscript received 20 December 2019; published 16 January 2020)

Recent evidence from magnetic torque, electron spin resonance, and second harmonic generation indicate that the prototypical quantum spin liquid candidate, herbertsmithite, has a symmetry lower than its x-ray refined trigonal space group. Here we consider known and possible distortions of this mineral class, along with related copper kagome oxides and fluorides, relate these to possible valence bond patterns, and comment on their relevance to the physics of these interesting materials.

DOI: [10.1103/PhysRevResearch.2.013055](https://doi.org/10.1103/PhysRevResearch.2.013055)

The nature of the ground state of the nearest-neighbor antiferromagnetic Heisenberg model on a kagome lattice (KAHM) has proven to be a challenging problem. Numerical simulations indicate that a variety of different states have comparable energies, including gapped spin liquids, gapless spin liquids, and valence bond solids. This is reflected in the energy spectrum of clusters from exact diagonalization studies, which shows a dense array of excited states extending down to zero energy [1]. In real materials, further richness emerges due to the presence of anisotropic interactions, such as Dzyaloshinskii-Moriya, as well as longer-range exchange. In this context, the lack of observation of an ordered ground state down to 20 mK in herbertsmithite, $\text{ZnCu}_3(\text{OH})_6\text{Cl}_2$, a mineral where copper ions sit on a perfect kagome lattice, has been a significant result [2–4].

In reality, though, herbertsmithite is far from perfect. Single crystals typically contain 15% of copper ions sitting on interlayer sites nominally occupied by zinc [5]. Moreover, despite x-ray refinements of the crystal structure which indicate perfect trigonal symmetry ($R\bar{3}m$), magnetic torque and electron spin resonance [6] find a breaking of the threefold trigonal axis. This has been recently amplified by second-harmonic-generation (SHG) data, which is consistent with a monoclinic space group that breaks inversion [7].

To put these results in context, it is first helpful to review known distortions in this mineral class, as well as related materials. The $\text{Cu}_4(\text{OH})_6\text{Cl}_2$ polymorph from which herbertsmithite arises via Zn substitution for Cu, $\text{Zn}_x\text{Cu}_{4-x}(\text{OH})_6\text{Cl}_2$, is clinoptacumite with a monoclinic $P2_1/n$ space group [8]. On Zn doping, an intermediate $R\bar{3}$ phase (Zn-paratacamite) is stabilized between $R\bar{3}m$ at high temperatures and $P2_1/n$

at low temperatures. Eventually, the $P2_1/n$ phase disappears, and then for x beyond about 0.34, so does the $R\bar{3}$ phase [9]. For Mg-paratacamite, the $R\bar{3}$ phase has been detected up to $x = 0.62$ [10]. To understand the nature of these two structural phases, we employ the crystallographic tools AMPLIMODES [11] and ISODISTORT [12].

The $R\bar{3}$ phase is driven by an F_2^+ distortion mode resulting in a quadrupling of the unit cell in the planar directions [Fig. 1 (left)]. Here F is equal to $(0, \frac{1}{2}, 1)$ in hexagonal reciprocal lattice units and is related to the $M(\frac{1}{2}, 0, 0)$ point of the hexagonal zone (the difference from M reflects the ABC stacking of layers in the rhombohedral lattice). The resulting crystallographic distortion from the F_2^+ mode is shown in Fig. 2. Basically, the interlayer sites (which would nominally be occupied by Zn in stoichiometric herbertsmithite) divide into two sets, one showing octahedral coordination (1/4 of these sites) and the other a Jahn-Teller distorted 2+2+2 coordination (the remainder). Around the first type, the atoms on the kagome plane rotate about it. This is known as a polar vortex [15] (more formally, an axial toroidal dipole [16]). The distortion pattern around the other interlayer sites has aspects of this as well but is more complicated. The actual crystal structure is even more complicated, given the presence of F_1^+ and Γ_2^+ secondary modes [Fig. 1 (left)]. Looking at just the copper kagome sites [17], one finds two crystallographically distinct sites. This leads to a distribution of Cu-Cu kagome distances. The strongest singlet bond (largest Cu-O-Cu bond angle, the superexchange scaling with the bond angle [18]) forms a pinwheel pattern, as shown in Fig. 3 (left). This same pattern is seen in copper kagome fluorides such as $\text{Rb}_2\text{Cu}_3\text{SnF}_{12}$ [19]. Such a pinwheel valence bond pattern has been previously discussed in the KAHM literature given its favorable energetics [20]. Note that this phase differs subtly from the so-called diamond valence bond solid, as resonances around diamonds would take one outside of the ground-state manifold [21] since those other bonds are not equivalent to the strong bonds. That is, because of the lattice distortion, there is an exchange energy cost for a diamond resonance that can be estimated as $2(J_{12} - J_{11} - J_{22})$, where J_{12} is the superexchange of the strong bond and 1 and 2 refer to the two crystallographically

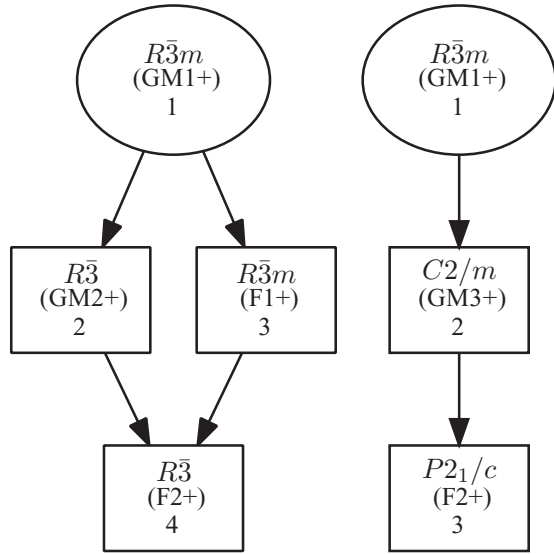


FIG. 1. Group-subgroup relation leading to (left) $R\bar{3}$ and (right) $P2_1/c$ (equivalent to $P2_1/n$) [13]. As indicated in these graphs, the primary distortion mode is F_2^+ , and the secondary modes, arising from the intermediate groups, are Γ_2^+ and F_1^+ for $R\bar{3}$ and Γ_3^+ for $P2_1/c$.

distinct kagome sites. For a resonance around a pinwheel, the energy cost is $6(J_{12}-J'_{12})$, where J'_{12} refers to the 1-2 bond with the smaller Cu-O-Cu bond angle. Given the linear relation of J with the Cu-O-Cu bond angle for the bond angle range appropriate to these materials [18,22,23], the estimated cost of a diamond resonance is $0.54J_{12}$ and a pinwheel resonance $1.45J_{12}$ for $x = 0.29$ [9]. These differences become much smaller as x increases (for Mg-paratacamite at $x = 0.62$, they become $0.03J_{12}$ and $0.02J_{12}$, respectively [10]).

The related $P2_1/n$ phase seen in clinoatacamite also arises from an F_2^+ distortion mode, the difference being due to different secondary modes [Γ_3^+ only for $P2_1/n$; Fig. 1 (right)]. The change in the overall distortion pattern leads to the strong bond now having a herringbone-like structure [Fig. 3 (right)].

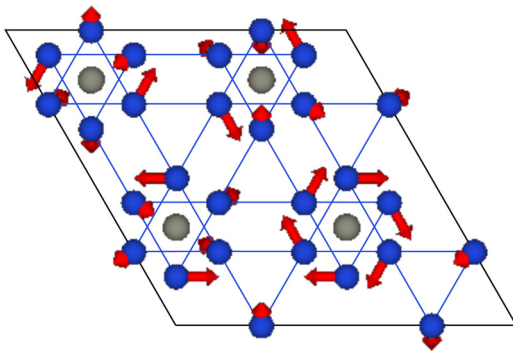


FIG. 2. F_2^+ distortion mode for the $R\bar{3}$ phase of Zn-paratacamite [9] from AMPLIMODES [11] plotted using VESTA [14]. Only the copper/zinc ions are shown in an intersite plane and the two kagome planes that sandwich it (blue kagome, gray intersite). Note the vortexlike motion of the kagome coppers about one of the intersites. This occurs as well for the oxygen, hydrogen, and chlorine ions (not shown).

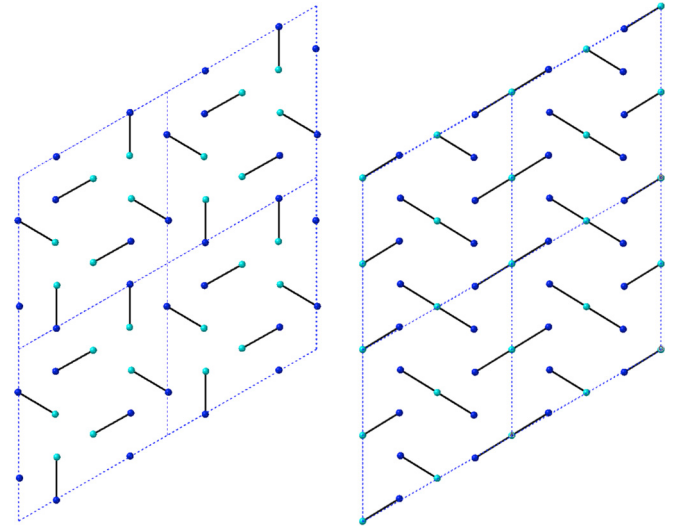


FIG. 3. Valence bond patterns for (left) the $R\bar{3}$ phase (Zn-paratacamite) and (right) the $P2_1/n$ phase (clinoatacamite). Similar patterns are seen for the $P6_3/m$ and $Pnma$ phases of barlowite, respectively. Only the copper ions are shown in a single kagome plane (the two crystallographically distinct sites are in blue and cyan).

This has previously been commented on in regards to the $Pnma$ distortion seen in the closely related material, barlowite, $Cu_4(OH)_6BrF$ [24]. The distortion in the latter case is an M_2^+ mode due to the difference in stacking (AA), the high-symmetry phase being hexagonal ($P6_3/mmc$). In fact, there is a close analogy between the phase transitions seen in weakly Zn-doped clinoatacamite ($R\bar{3}m$ to $R\bar{3}$ to $P2_1/n$) and barlowite ($P6_3/mmc$ to $P6_3/m$ to $Pnma$). In the former case, the primary distortion mode is F_2^+ with secondary modes F_1^+ and Γ_2^+ ($R\bar{3}$) and Γ_3^+ ($P2_1/n$). For the latter, the primary distortion mode is M_2^+ with secondary modes M_1^+ and Γ_2^+ ($P6_3/m$) and Γ_5^+ ($Pnma$). These differences again are due to ABC stacking (rhombohedral) versus AA stacking (hexagonal). This is summarized in Table I.

The detailed temperature dependence of these distortions has been considered by Malcherek *et al.* for clinoatacamite [25] and Welch *et al.* for Zn-paratacamite [9]. The resulting analysis from AMPLIMODES is shown in Fig. 4. Despite the expected first-order nature of the $R\bar{3}$ to $P2_1/n$ phase transition, one sees that the F_2^+ distortion amplitude goes smoothly through the transition, and to a good approximation follows a Landau mean-field behavior of $\sqrt{T_{s1} - T}$, where T_{s1} is the upper transition. Given the limited data, it is hard to quantify the T dependence of the secondary modes. Nominally, the amplitude of the Γ_3^+ mode should be quadratic in F_2^+ , but in reality it sets in discontinuously at T_{s2} (lower transition) due to the finite value of F_2^+ at T_{s2} .

Returning to the valence bond patterns, a pinwheel pattern is also found in the higher-symmetry ($P6_3/m$) version of barlowite [24] (consistent with the above-discussed analogy with Zn-paratacamite) as also listed in Table I. The known list of patterns can be expanded by considering other materials in the class $A_2Cu_3BF_{12}$ where A is an alkali metal and B a 4+ cation [31]. These are also listed in Table I. In particular,

TABLE I. Known valence bond solid (VBS) patterns in copper kagome materials. “Low T ” is the low-temperature crystal structure, and “High T ” the high-temperature one. “Mode” is the primary distortion mode. z indicates the net buckling of the copper ions in the kagome plane along the hexagonal c axis (in Å). The high- T phase of $\text{Cs}_2\text{Cu}_3\text{CeF}_{12}$ is unknown and so was determined from group-subgroup relations. Note the large buckling often present in the copper fluorides as compared to the copper hydroxychlorides. References are clinoatacamite [25], paratacamite [9], barlowite [24], averievite [26], $\text{Cs}_2\text{Cu}_3\text{CeF}_{12}$ [27], $\text{Cs}_2\text{Cu}_3\text{ZrF}_{12}$ [28], $\text{Cs}_2\text{Cu}_3\text{SnF}_{12}$ [29], and $\text{Rb}_2\text{Cu}_3\text{SnF}_{12}$ [30].

| Low T | High T | VBS | Material | Mode | z |
|------------------------|----------------------------|-------------|---|----------------|--------------|
| $\text{P2}_1/\text{n}$ | $\text{R}\bar{3}\text{m}$ | herringbone | clinoatacamite $\text{Cs}_2\text{Cu}_3\text{SnF}_{12}$ | F_2^+ | 0.07 0.07 |
| $\text{P2}_1/\text{c}$ | $\text{P}\bar{3}\text{m1}$ | herringbone | averievite | M_2^+ | 0.00 |
| Pnma | $\text{P6}_3/\text{mmc}$ | herringbone | barlowite (1) | M_2^+ | 0.07 |
| $\text{R}\bar{3}$ | $\text{R}\bar{3}\text{m}$ | pinwheel | paratacamite $\text{Rb}_2\text{Cu}_3\text{SnF}_{12}$ | F_2^+ | 0.06 0.38 |
| $\text{P6}_3/\text{m}$ | $\text{P6}_3/\text{mmc}$ | pinwheel | barlowite (2) | M_2^+ | 0.06 |
| $\text{P2}_1/\text{m}$ | $\text{R}\bar{3}\text{m}$ | zigzag | $\text{Cs}_2\text{Cu}_3\text{ZrF}_{12}$ | F_2^- | 0.73 |
| Pnnm | $\text{P6}_3/\text{mmc}$ | stripe | $\text{Cs}_2\text{Cu}_3\text{CeF}_{12}$ | M_3^+ | 3.93 |

one also finds stripe phases ($\text{Cs}_2\text{Cu}_3\text{CeF}_{12}$) and zigzag phases ($\text{Cs}_2\text{Cu}_3\text{ZrF}_{12}$). In all cases in Table I, though, inversion symmetry is preserved.

This brings us to the SHG data on herbertsmithite [7]. They indicate a point group of either 2 or m . A likely candidate, then, for the inversion-breaking space group is either Cm or C2 . There are two ways this can happen. The first is by condensing a zone-centered polar mode (Γ_3^- , Fig. 5). Possible valence bond patterns are shown in Fig. 6. Another way is by condensing an F-centered mode (Fig. 7) as shown in Fig. 8 (note, though, that the F_2^- example given in Table I

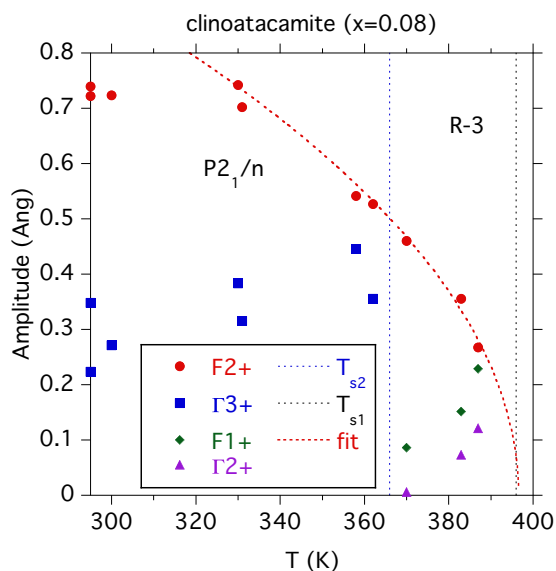


FIG. 4. Temperature dependence of the distortion mode amplitudes (in Å) from clinoatacamite [25] generated by AMPLIMODES [11]. The red dashed curve is a Landau mean-field fit to the F_2^+ mode.

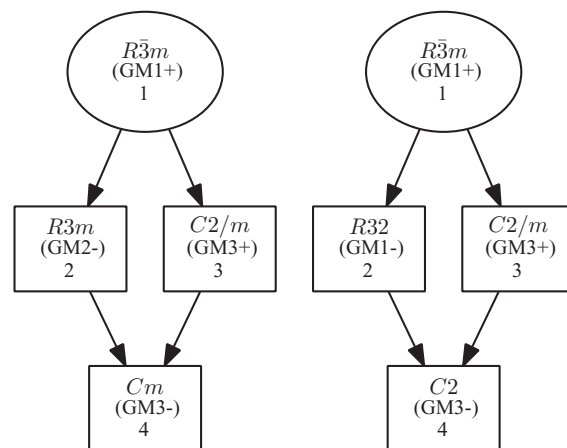


FIG. 5. Group-subgroup relation leading to (left) Cm and (right) C2 , driven by a Γ -centered primary mode [13]. As indicated in these graphs, the primary mode is Γ_3^- , and the secondary modes, arising from the intermediate groups, are Γ_2^- and Γ_3^+ for Cm and Γ_1^- and Γ_3^+ for C2 .

preserves inversion). Again, these can take the form of stripes or zigzags, some of which result from buckled planes. Note that for illustrative purposes, these patterns are based on the shortest Cu-Cu bonds. In reality, the strongest singlets will depend on the Cu-O-Cu bond angles, meaning oxygen atom displacements need to be considered once they are known. But one important difference to realize is that for the zone-centered case, one maintains an odd number of copper ions (per plane) in the unit cell. Therefore, we would anticipate an anisotropic spin liquid in this case rather than a valence bond solid [32]. For the zone-boundary modes, though, the unit cell size increases, resulting in an even number of copper ions instead, so this would be a valence bond solid.

One interesting point about the Cm and C2 space groups is that they are in general ferroelectric, with the polar axis

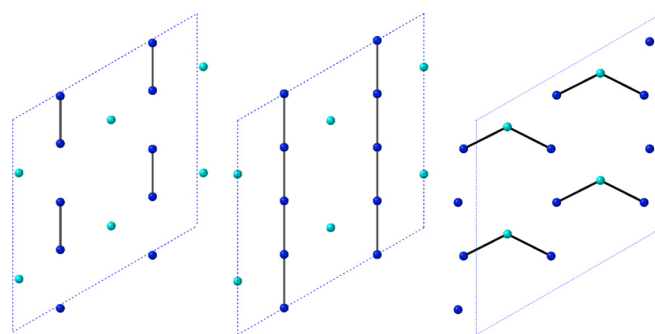


FIG. 6. Various Cm and C2 VBS patterns from a zone-centered mode (Γ_3^-) generated by ISODISTORT [12]. Left: Cm B_{u1} pattern; middle: Cm B_{u2} pattern; right: C2 A_u pattern. Here A_u and B_u refer to point group symmetries of the copper kagome ions. The Cm A_u pattern (not shown) is similar to the Cm B_{u1} one. These patterns are based on just copper-kagome-ion displacements and the shortest Cu-Cu bonds (only the copper ions are shown in a single kagome plane; the two crystallographically distinct sites are in blue and cyan). The actual pattern will depend on the Cu-O-Cu bond angles once oxygen-ion displacements are known.

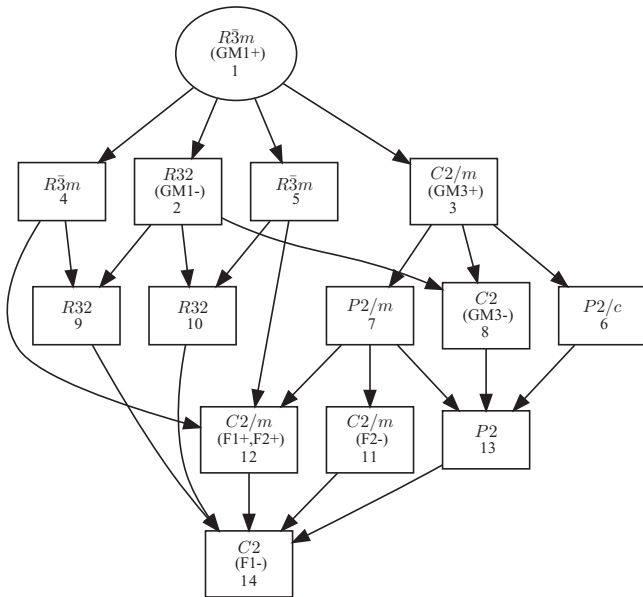
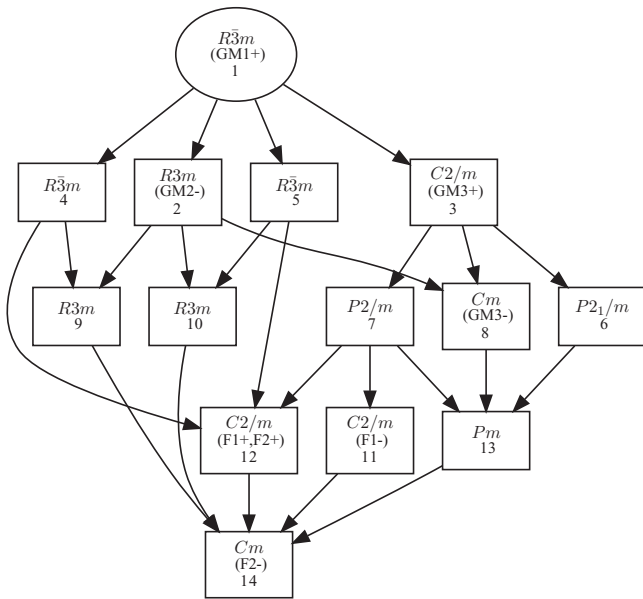


FIG. 7. Group-subgroup relation leading to (top) Cm and (bottom) C2, driven by an F-centered primary mode [13]. As indicated in these graphs, the primary mode is F_2^- for Cm and F_1^- for C2, with a variety secondary modes, arising from the intermediate groups, that differ for Cm and C2.

along the twofold (hexagonal b axis) for C2 and perpendicular to this axis for Cm. Ferroelectric behavior has been claimed for the cobalt analog of clinoatacamite, with a proposed structural distortion of $R\bar{3}m$ [33]. Indications of ferroelectric-like behavior has also been seen in averievite [34], where a transition from the intermediate $P2_1/c$ phase to a lower-temperature phase of unknown symmetry has been observed [26]. This brings up the question of spin-lattice coupling. The SHG signal in herbertsmithite follows the predicted temperature dependence of the spin-spin correlator for a kagome lattice [7]. This is consistent with the temperature dependence of phonon linewidths [35]. Moreover, the phonon frequen-

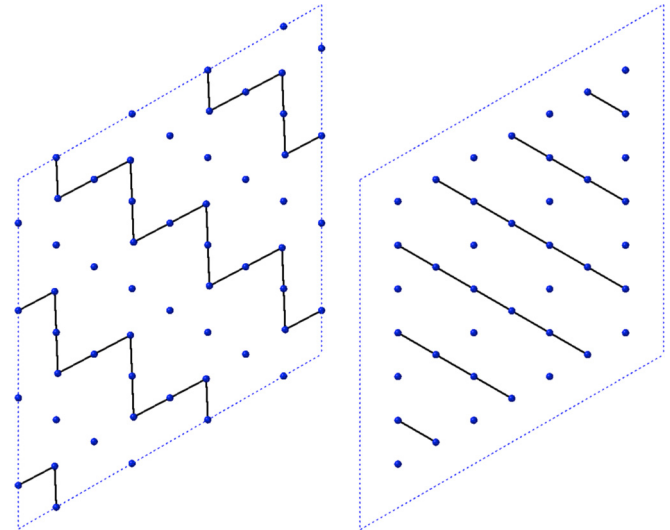


FIG. 8. Two of the Cm VBS patterns from a zone-boundary mode (F_2^-) generated by ISODISTORT [12]. Left: One of the two B_{u1} patterns; right: One of the two B_{u2} patterns. The other two patterns are dimer patterns similar to Fig. 6(a). These patterns are based on just copper-kagome-ion displacements and the shortest Cu-Cu bonds (only the copper ions are shown in a single kagome plane; there are seven crystallographically distinct sites). The actual pattern will depend on the Cu-O-Cu bond angles once oxygen-ion displacements are known.

cies shift [35], also indicative of spin-lattice coupling as has been studied extensively in pyrochlores [36,37]. The idea here is that the superexchange J is sensitive to distortions given its dependence on the Cu-O-Cu bond angle, harking back to early work by Baltensperger [38], with the distortion occurring if the gain in exchange energy from increasing the bond angle exceeds the elastic cost of the lattice distortion. Spin-lattice couplings have been quantified in clinoatacamite using Raman data [39]. Ultimately, they can lead to multiferroic behavior, as observed in the distorted kagome material $KCu_3As_2O_7(OH)_3$ [40].

Finally, what does all of this have to do with the KAHM? Density matrix renormalization group simulations have indicated that the ground state is a melted version of a 12-site diamond valence bond solid, closely related to the pinwheel pattern [41]. This has been further investigated by more recent numerical work [42], though related numerical simulations favor a Dirac spin liquid instead [43–45]. Small perturbations could certainly stabilize a valence bond solid [46–48], or an anisotropic spin liquid [32,49]. Given the above results, such models should be further explored to understand the rich physics of the Heisenberg model on a kagome lattice and its material realizations.

M.R.N. was supported by the Materials Sciences and Engineering Division, Basic Energy Sciences, Office of Science, U.S. Department of Energy. N.J.L. acknowledges partial support from an Institute for Quantum Information and Matter Postdoctoral Fellowship. D.H. acknowledges support from ARO PECASE Award No. W911NF-17-1-0204.

- [1] P. Lecheminant, B. Bernu, C. Lhuillier, L. Pierre, and P. Sindzingre, *Phys. Rev. B* **56**, 2521 (1997).
- [2] M. P. Shores, E. A. Nytko, B. M. Bartlett, and D. G. Nocera, *J. Am. Chem. Soc.* **127**, 13462 (2005).
- [3] P. Mendels and F. Bert, *J. Phys. Soc. Jpn.* **79**, 011001 (2010).
- [4] M. R. Norman, *Rev. Mod. Phys.* **88**, 041002 (2016).
- [5] T. H. Han, J. S. Helton, S. Chu, A. Prodi, D. K. Singh, C. Mazzoli, P. Muller, D. G. Nocera, and Y. S. Lee, *Phys. Rev. B* **83**, 100402(R) (2011).
- [6] A. Zorko, M. Herak, M. Gomilsek, J. van Tol, M. Velazquez, P. Khuntia, F. Bert, and P. Mendels, *Phys. Rev. Lett.* **118**, 017202 (2017).
- [7] N. J. Laurita, A. Ron, J. W. Han, A. Scheie, J. P. Sheckelton, R. W. Smaha, W. He, J.-J. Wen, J. S. Lee, Y. S. Lee, M. R. Norman, and D. Hsieh, [arXiv:1910.13606](https://arxiv.org/abs/1910.13606).
- [8] J. D. Grice, J. T. Szymanski, and J. L. Jambor, *Can. Mineral.* **34**, 73 (1996).
- [9] M. D. Welch, M. J. Sciberras, P. A. Williams, P. Leverett, J. Schluter, and T. Malcherek, *Phys. Chem. Miner.* **41**, 33 (2014).
- [10] A. R. Kampf, M. J. Sciberras, P. Leverett, P. A. Williams, T. Malcherek, J. Schluter, M. D. Welch, M. Dini, and A. A. M. Donoso, *Mineral. Mag.* **77**, 3113 (2013).
- [11] D. Orobengoa, C. Capillas, M. I. Aroyo, and J. M. Perez-Mato, *J. Appl. Crystallogr.* **42**, 820 (2009).
- [12] B. J. Campbell, H. T. Stokes, D. E. Tanner, and D. M. Hatch, *J. Appl. Crystallogr.* **39**, 607 (2006).
- [13] S. Ivantchev, E. Kroumova, G. Madariaga, J. M. Perez-Mato, and M. I. Aroyo, *J. Appl. Crystallogr.* **33**, 1190 (2000).
- [14] K. Momma and F. Izumi, *J. Appl. Crystallogr.* **44**, 1272 (2011).
- [15] A. K. Yadav, C. T. Nelson, S. L. Hsu, Z. Hong, J. D. Clarkson, C. M. Schlepueetz, A. R. Damodaran, P. Shafer, E. Arenholz, L. R. Dedon, D. Chen, A. Vishwanath, A. M. Minor, L. Q. Chen, J. F. Scott, L. W. Martin, and R. Ramesh, *Nature* **530**, 198 (2016).
- [16] V. M. Dubovik, L. A. Tosunyan, and V. V. Tugushev, *Zh. Eksp. Teor. Fiz.* **90**, 590 (1986) [*Sov. Phys. JETP* **63**, 344 (1986)].
- [17] For simplicity, in this paper we focus on copper-ion displacements. Oxygen-ion displacements play an equally important role as indicated later. Which one dominates does not affect the definition of primary versus secondary modes, which is set by the group-subgroup relations and resulting Landau free energy, though the nature of the ion displacements depends critically on the symmetry of these modes.
- [18] V. H. Crawford, H. W. Richardson, J. R. Wasson, D. J. Hodgson, and W. E. Hatfield, *Inorg. Chem.* **15**, 2107 (1976). The linear relation of J with Cu-O-Cu bond angle for copper hydroxides is such that the critical angle (where $J = 0$) is 97.54° .
- [19] K. Matan, T. Ono, Y. Fukumoto, T. J. Sato, J. Yamaura, M. Yano, K. Morita, and H. Tanaka, *Nat. Phys.* **6**, 865 (2010).
- [20] B.-J. Yang and Y. B. Kim, *Phys. Rev. B* **79**, 224417 (2009).
- [21] A. Wietek and A. M. Lauchli, [arXiv:1908.02762](https://arxiv.org/abs/1908.02762).
- [22] X. Rocquefelte, K. Schwarz, and P. Blaha, *Sci. Rep.* **2**, 759 (2012).
- [23] Y. Iqbal, H. O. Jeschke, J. Reuther, R. Valentí, I. I. Mazin, M. Greiter, and R. Thomale, *Phys. Rev. B* **92**, 220404(R) (2015).
- [24] R. W. Smaha, W. He, J. M. Jiang, C. J. Titus, J. Wen, Y.-F. Jiang, J. P. Sheckelton, S. G. Wang, Y.-S. Chen, S. J. Teat, A. A. Aczel, Y. Zhao, G. Xu, J. W. Lynn, H.-C. Jiang, and Y. S. Lee, [arXiv:1907.00454](https://arxiv.org/abs/1907.00454).
- [25] T. Malcherek, B. Mihailova, and M. D. Welch, *Phys. Chem. Miner.* **44**, 307 (2017).
- [26] A. S. Botana, H. Zheng, S. H. Lapidus, J. F. Mitchell, and M. R. Norman, *Phys. Rev. B* **98**, 054421 (2018).
- [27] T. Amemiya, M. Yano, K. Morita, I. Umegaki, T. Ono, H. Tanaka, K. Fujii, and H. Uekusa, *Phys. Rev. B* **80**, 100406(R) (2009).
- [28] S. A. Reisinger, C. C. Tang, S. P. Thompson, F. D. Morrison, and P. Lightfoot, *Chem. Mater.* **23**, 4234 (2011).
- [29] L. J. Downie, C. Black, E. I. Ardashnikova, C. C. Tang, A. N. Vasiliev, A. N. Golovanov, P. S. Berdonosov, V. A. Dolgikh, and P. Lightfoot, *CrystEngComm* **16**, 7419 (2014).
- [30] L. J. Downie, S. P. Thompson, C. C. Tang, S. Parsons, and P. Lightfoot, *CrystEngComm* **15**, 7426 (2013).
- [31] K. Matan, T. Ono, G. Gitgeatpong, K. de Roos, P. Miao, S. Torii, T. Kamiyama, A. Miyata, A. Matsuo, K. Kindo, S. Takeyama, Y. Nambu, P. Piyawongwatthana, T. J. Sato, and H. Tanaka, *Phys. Rev. B* **99**, 224404 (2019).
- [32] B. K. Clark, J. M. Kinder, E. Neuscamman, Garnet Kin-Lic Chan, and M. J. Lawler, *Phys. Rev. Lett.* **111**, 187205 (2013).
- [33] X.-L. Xu, D.-D. Meng, X.-G. Zheng, I. Yamauchi, I. Watanabe, and Q.-X. Guo, *Phys. Rev. B* **95**, 024111 (2017).
- [34] T. Biesner, A. Pustogow, H. Zheng, J. F. Mitchell, and M. Dressel (unpublished).
- [35] A. B. Sushkov, G. S. Jenkins, T.-H. Han, Y. S. Lee, and H. D. Drew, *J. Phys.: Condens. Matter* **29**, 095802 (2017).
- [36] Y. Yamashita and K. Ueda, *Phys. Rev. Lett.* **85**, 4960 (2000).
- [37] A. B. Sushkov, O. Tchernyshyov, W. Ratcliff II, S. W. Cheong, and H. D. Drew, *Phys. Rev. Lett.* **94**, 137202 (2005).
- [38] H. Baltensperger and J. S. Helman, *Helv. Phys. Acta* **41**, 668 (1968).
- [39] X.-D. Liu, X.-G. Zheng, D.-D. Meng, X.-L. Xu, and Q.-X. Guo, *J. Phys.: Condens. Matter* **25**, 256003 (2013).
- [40] G. J. Nilsen, Y. Okamoto, H. Ishikawa, V. Simonet, C. V. Colin, A. Cano, L. C. Chapon, T. Hansen, H. Mutka, and Z. Hiroi, *Phys. Rev. B* **89**, 140412(R) (2014).
- [41] S. Yan, D. A. Huse, and S. R. White, *Science* **332**, 1173 (2011).
- [42] A. Ralko, F. Mila, and I. Rousochatzakis, *Phys. Rev. B* **97**, 104401 (2018).
- [43] Y. Ran, M. Hermele, P. A. Lee, and X.-G. Wen, *Phys. Rev. Lett.* **98**, 117205 (2007).
- [44] Y. Iqbal, D. Poilblanc, and F. Becca, *Phys. Rev. B* **89**, 020407(R) (2014).
- [45] Y.-C. He, M. P. Zalatel, M. Oshikawa, and F. Pollmann, *Phys. Rev. X* **7**, 031020(R) (2017).
- [46] Y. Huh, M. Punk, and S. Sachdev, *Phys. Rev. B* **84**, 094419 (2011).
- [47] Y. Iqbal, F. Becca, and D. Poilblanc, *New J. Phys.* **14**, 115031 (2012).
- [48] K. Hwang, Y. Huh, and Y. B. Kim, *Phys. Rev. B* **92**, 205131 (2015).
- [49] C. Repellin, Y.-C. He, and F. Pollmann, *Phys. Rev. B* **96**, 205124 (2017).